PbS Quantum-dots in Glasses

Chao Liu and Jong Heo*

Center for Information Materials, Department of Materials Science and Engineering, Pohang University of Science and Technology, Pohang, Gyeongbuk 790-784, Korea

**E-mail: jheo@postech.ac.kr*

Abstract: PbS QDs in glasses have attracted much attention due to the potentials for near-infrared applications. Growth of PbS QDs in the glass is discussed and size of PbS QDs formed in the glass can be tuned by varying the thermal treatment conditions. Hyperbolic-band approximation and four-band envelope function provide good simulation of the exciton energies of PbS QDs. Absorption and photoluminescence of PbS QDs was tuned into 1~2 μm wavelength regime with large full width at half maximum photoluminescence intensity (>160 nm). Photoluminescence intensity of PbS QDs in the glasses was closely related to size of quantum dots, temperature, excitation and defects. Decrease in temperature shifted the photoluminescence bands to shorter wavelength and switched the photoluminescence from darkened state and brightened state.

1. Introduction

Semiconductor nanocrystals (Quantum dots or QDs) have attracted attention due to the unique optical and electronic properties induced by the quantum confinement effect[1,2]. When the size of semiconductor nanocrystals is comparable to or smaller than the Bohr exciton radius, the energy gap of semiconductor nanocrystals increases and the energy spectrum becomes discrete. Among various quantum dots, IV-VI quantum dots made of PbS, PbSe and PbTe have attracted attention recently[3-5]. Bulk IV-VI semiconductor materials have narrow band gap energies, 0.41 eV for PbS and 0.28 eV for PbSe, and large Bohr exciton radii, 18 and 46 nm for PbS and PbSe, respectively. Thus, the strong confinement effect can easily be achieved with a moderate quantum dot size. In addition, effective band gap energies of these quantum dots can be tuned in a wide range, covering the visible and near infrared spectral regime. Therefore, IV-VI quantum dots are not only useful for the investigation of strong quantum confinement effect, but also for near infrared lasers[3], broadband optical amplifiers[4] and solar cells[5].

PbS nanocrystals studied either inside the colloidal solutions[6,7], or in transparent solid media[8-10]. Colloidal chemistry is one of the most powerful methods to prepare quantum dots with high quantum efficiency[6,7]. However, it is necessary for these QDs to be embedded into solid matrices such as glasses to realize any commercial applications. Synthesis of quantum dots in glasses through nucleation and growth is particularly attractive since it is inexpensive and relatively easy to control the size of quantum dots. Glasses are also chemically durable with high mechanical strength. In addition, the versatility of glassy hosts allows fabrication of devices in the bulk, planar or fiber forms.

In this paper, PbS QDs embedded in glass matrices are reported. In section 2, the growth dynamics of PbS QDs in oxide glasses are examined. Section 3 is devoted to the electronic states of PbS QDs and section 4 deals with the optical properties of PbS QDs in glasses along with the effects of quantum dots size, defects and temperatures.

2. Synthesis and Characterization

Several techniques have been developed to prepare PbS QDs in glasses including solid-state precipitation[11], ion-implantation[12] and sol-gel process[13]. Solid-state precipitation has long been used to synthesize semicon-

ductor nanocrystals. In general, precursor glasses containing semiconductor materials were prepared by melt-quenching methods, and subsequent heat-treatment at the temperature near the glass transition resulted in the formation of semiconductor quantum dots. Fig. 1 shows the typical high resolution TEM image of a PbS quantum dot precipitated in borosilicate glasses by the thermal treatment. The quality of PbS QDs thus formed was comparable to those synthesized through colloidal chemistry. Silicate glasses, borosilicate glasses and phosphate glasses were frequently used as the precursors, and the maximum lead chalcogenide concentrations were estimated to be ~0.1 at% in borosilicate glasses[14] and below 1.0 at% in phosphate glasses[15].

Growth of quantum dots in glasses is based on the thermodynamics of diffusion-controlled phase decomposition of over-saturated solid solutions. The annealing temperature should be high enough to initiate the effective diffusion of semiconductor ions and at the same time, low enough to maintain the over-saturation in the solutions. These processes are divided into three stages: nucleation, growth and coalescence[16]. During the nucleation process, the critical nucleus size is described by the following expression[17]:

$$a_{cr} = 2\sigma T_0 \upsilon / H(T_0 - T) \quad (1)$$

where, a_{cr} is the critical size of nuclei, and is the coefficient related to the interfacial surface tension. T is the annealing temperature, and T_0 is the temperature of equilibrium solution. υ is the specific volume of the particle H and is the mean specific enthalpy. During the diffusion-controlled growth process, the size of the crystals can be described as[16]:

$$a = (2(C_0 - C_e)/(C_P - C_e))^{1/2}(D\tau)^{1/2} \quad (2)$$

where, a is the mean radius of the particles, τ is the time of annealing, C_0 is the initial concentration of semiconductor phase and C_e is the equilibrium concentration of the phase in the particle. $D = D_0 \exp(\delta E/\kappa T)$ is the diffusion coefficient. In the coalescence process, the size of crystal changes as[18]:

$$a = (4\sigma/9)^{1/3}(D\tau)^{1/3} \quad (3)$$

where, σ is the coefficient related to the interfacial surface tension.

Since it is difficult to find the specific nucleation and growth temperatures, thermal treatment is generally

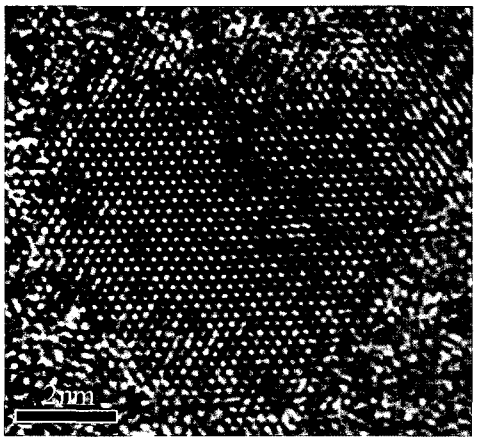

Fig. 1. High resolution transmission electron microscope image of PbS quantum dot in BZ glass heat-treated at 600℃ for 50 h.

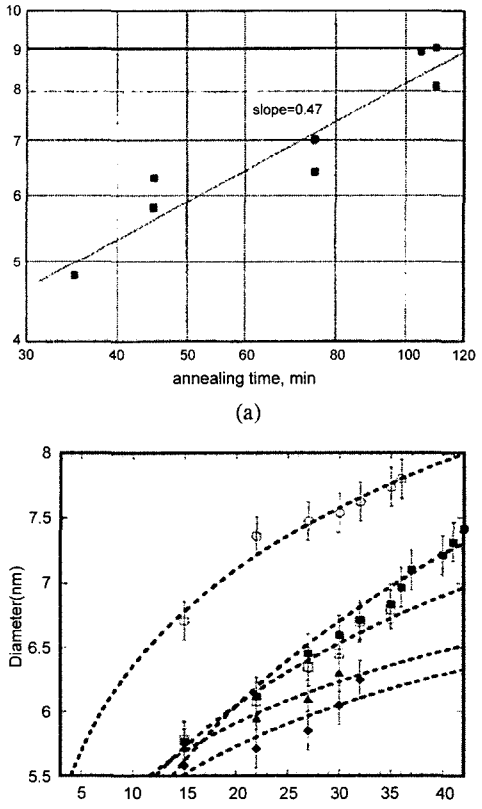

(a)

Fig. 2. (a) Diameter of PbS quantum dots formed in the phosphate glass versus the duration of annealing at T=405℃-square, and the results of the linear fitting[15]. (b) Evolution of the diameter of PbS QDs as a function of time at growth treatment temperatures ranging between 650 and 700℃[19].

conducted at temperatures near the glass transition. Fig. 2 shows the size of PbS quantum dots in phosphate[15] and borosilicate[19] glasses as a function of annealing time. In phosphate glass shown in Fig. 2(a), the time dependence of quantum dot size is close to the $t^{1/2}$, typical for the diffusion-controlled growth of independent nuclei[20]. On the other hand, growth of PbS quantum dots in borosilicate glasses follows $\sim t^{0.15\text{-}0.2}$ dependence at the early stage of crystal growth as shown in Fig. 2 (b). Diffusion controlled crystal growth and coalescence have $t^{1/2}$ and $t^{1/3}$ dependence, respectively as shown in Eqs. (2) and (3). Therefore, the sublinear time dependence indicates that coalescence process occurs at the early stage of the growth of PbS quantum dots. Different time dependences in the growth of PbS quantum dots from phosphate and borosilicate glass is not surprising, because the maximum concentrations of lead chalcogenide in these two glasses are different. Compared to phosphate glasses, borosilicate glasses can dissolve small concentration of PbS, thus the Pb and S required for the growth are depleted from the glass matrix at the early stage of growth, forcing the system into the coalescence regime[19].

Careful selection of thermal treatment temperature and time will yield quantum dots of desired sizes. High temperature and prolonged thermal treatment result in the formation of large quantum dots. Diffusion controlled growth of quantum dots yields narrower size dispersion compared to coalescence growth. For PbS QDs, size dispersion smaller than 10% has been achieved in glasses[11,19].

3. Electronic Structure

Several theoretical calculations have been developed to predict the electronic structures of PbS quantum dots. Representative examples are parabolic effective mass model[21,22], hyperbolic-band approximation[22], tight-binding model[22,23] and an envelope wave-function calculation[24]. Predictions of band gap energy using the first three models are schematically shown in Fig. 3.

For the parabolic effective mass approximation, the effective band gap energy can be expresses as[22]:

$$\Delta E = \frac{\hbar^2\pi^2}{2R^2}\left(\frac{1}{m_e}+\frac{1}{m_h}\right)-\frac{1.8e^2}{\varepsilon R}+(\textit{polarization term}) \quad (4)$$

where, ΔE is the energy of the first excited state. The first term is the kinetic energies of the electron and hole that increase as the particle size decrease. The second term is the screened Coulomb interaction which stabilizes the electron-hole pair, and the third term is the polarization energy that is generally small. As shown in Fig. 3, prediction from this model started to deviate from the experimental values when the particle size became smaller than ~100 Å. This break down was due to the non-parabolicity of the band structure of lead salts near the L point, which is induced by the interband coupling. The hyperbolic band model predicted that band gap energy of PbS particles changed as[22]:

$$\Delta E = [E_g^2 + 2\hbar^2 E_g(\pi/r)^2/m^*]^{1/2} \quad (5)$$

where, E_g is the bandgap energy of bulk PbS crystals, r is the radius of PbS nanocrystals and $m^*(=0.085m_e)$ is the effective mass. This hyperbolic model can predict the exciton energies of PbS particles of size down to ~25 Å, as shown in Fig. 4. The tight-binding model[23] and a simpler cluster model[22] provide accurate values of the electronic levels of PbS quantum dots smaller than 5 nm.

Recently, Kang and Wise calculated the electronic structures of PbS and PbSe quantum dots using a four-band envelope function formalism[24]. This formalism

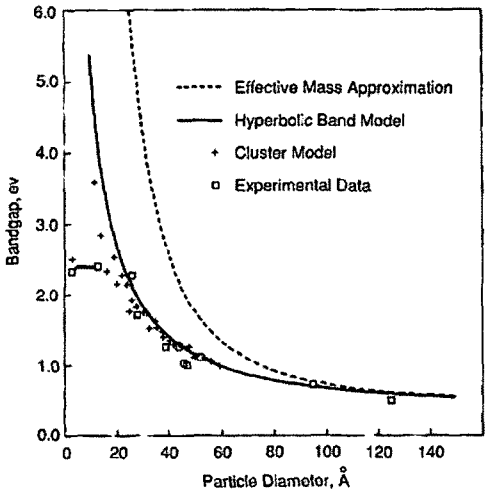

Fig. 3. Band gap energy of PbS as a function of particle size. □ represents experimental data, -□ indicates 13 Å is the upper limit. Dotted line is a theoretical calculation using the effective mass approximation, solid line is a theoretical calculation from hyperbolic band model, and + represents the calculation from the cluster model[22].

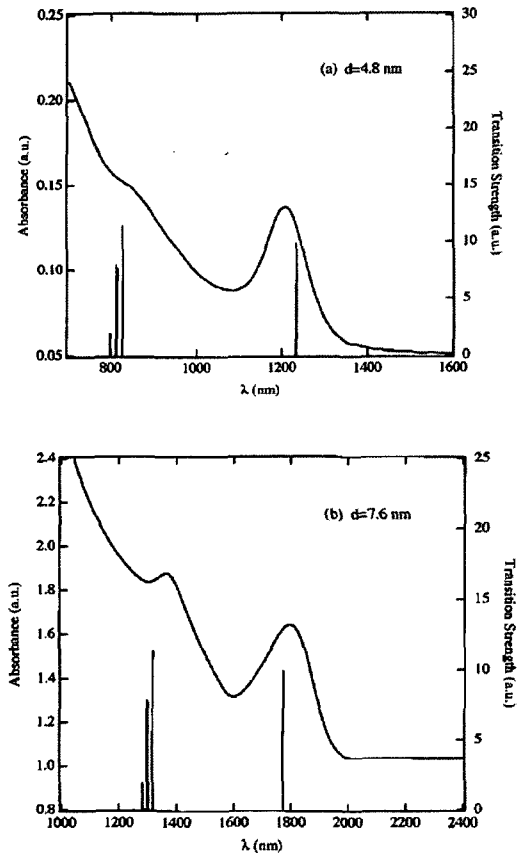

Fig. 4. Absorption spectra and calculated transition strengths of PbS QDs with diameters of (a) 4.8 nm and (b) 7.6 nm [24].

accounted for the exciton energies and wave functions with the correct symmetries of the materials. They were able to provide the energy spectrum and wave functions as well as dipole transition strengths and selection rules. Good agreement with the experimental band gap energies of PbS quantum dots down to 3 nm in diameter was achieved.

4. Optical Properties

4.1 Absorption spectrum

PbS QDs formed in the matrix manifested themselves as peaks in the absorption spectrum. Position of absorption peak was determined by the average size of quantum dots. Large size dispersion normally induces inhomogeneous broadening of the absorption spectrum, obscuring the exciton absorption peaks[25]. Furthermore, the nature of the matrix and shape of quantum dots also have significant effects on the absorption spectrum[26,27]. Fig. 5 shows typical absorption spectra of PbS quantum dots embedded in borosilicate glasses[28]. Increase in the duration or temperature of thermal treatment resulted in the shift of the absorption to the longer wavelength side. For BC glass ($66SiO_2$-$8B_2O_3$-$18K_2O$-4BaO-4CaO with additional $0.3PbS$-$0.1Er_2S_3$, in mol%), broad absorption bands occurred at 1070, 1200, 1200 nm for glasses heat-treated at 600°C for 20, 30 and 70 h, respectively. For BZ glass ($66SiO_2$-$8B_2O_3$-$18K_2O$-4BaO-4ZnO (BZ glass) with additional 1.0 PbS, in mol%), absorption bands appeared at 1150, 1180, 1460 and 1700 nm upon thermal treatment at 600°C for 20 and 40 h, 620 and 640°C for 20 h, respectively. Careful selection of thermal treatment condition yielded PbS QDs with absorption and photoluminescence bands spanning over the whole transmission window of silica fiber (1.2~1.7μm). In addition, typical value of absorption

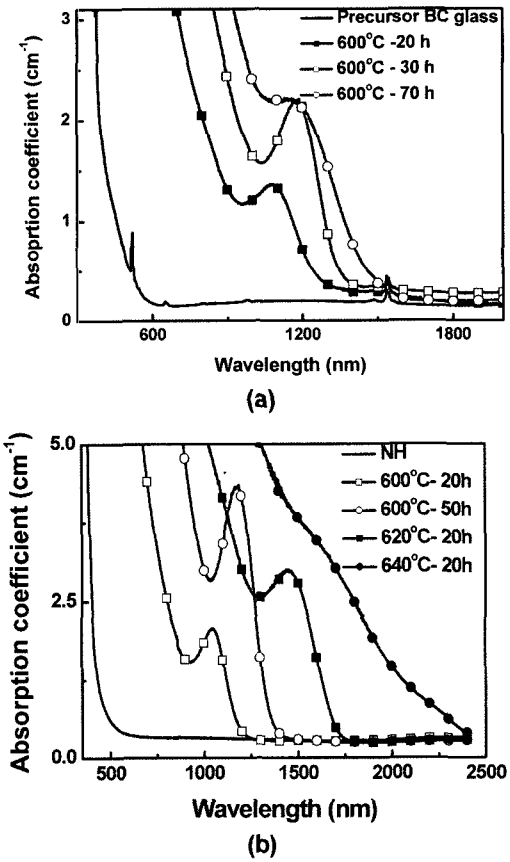

Fig. 5. Typical absorption spectra of PbS QDs in (a) BC glass and (b) BZ glass. Minor sharp absorption peaks in (a) was induced by the absorption of Er^{3+} ions.

cross-section of PbS QDs was $2\sim6\times10^{-17}cm^2$ [29], much larger than that of Er^{3+} ions (5×10^{-21} cm^2 at 1534 nm)[30]. These two features make PbS QDs doped glasses promising for broadband fiber-optic amplification.

4.2 Photoluminescence of PbS QDs

Upon excitation with above bandgap light, PbS quantum dots emitted photons in the visible or near infrared wavelength region, depending on the size of quantum dots. Fig. 6 shows the photoluminescence spectra of PbS QDs in BC and BZ glasses. Photoluminescence spectra of PbS QDs shifted to longer wavelength as their sizes increased, that agrees with the phenomenon observed in the absorption spectra. Estimated radius, effective bandgap energy, peak wavelength of photoluminescence (PL) and full width at half maximum (FWHM) luminescence intensity of PbS QDs embedded in BC and BZ glasses were summarized in Table 1.

Besides the effect of size of quantum dots, surface defects also have large influence on the photoluminescence properties. In PbS quantum dots, two kinds of defects have been reported, i.e., deep states in the energy gap due to excess Pb atoms at the interface and shallow states near the exciton level from the interstitial sulfur atoms[31]. As the size of the quantum dots decreases, the ratio of 'surface defects/volume atom' increases dramatically. These defects at the interface between the quantum dots and glass matrix act as traps for charge carriers. They seriously decrease the photoluminescence efficiency of quantum dots and in some cases, completely quench the photoluminescence through non-radiative decay. Due to the presence of defects on the surface of quantum dots, PbS QDs normally show low quantum efficiency. Thus, it is necessary to passivate the defect sites to optimize the photoluminescence, even though it appears difficult to achieve inside the glass matrix.

Table 1. Estimated Radius, Effective Bandgap Energy, Peak Wavelength of Photoluminescence (PL) and Full Width at Half Maximum (FWHM) Luminescence Intensity of PbS QDs Embedded in Different Glass Matrices

Glass	Heat-treatment condition	Radius (nm)	Effective bandgap energy (eV)	Peak wavelength of PL (nm)	FWHM (nm)
BC	600°C-20 h	2.5	1.05	1200	195
	600°C-30 h	2.7	0.94	1340	195
	600°C-70 h	3.0	0.87	1450	250
BZ	600°C-20 h	2.3	1.08	1166	160
	600°C-50 h	2.6	0.95	1318	180
	620°C-20 h	3.6	0.75	1620	200
	640°C-20 h	4.7	0.64	1680	500

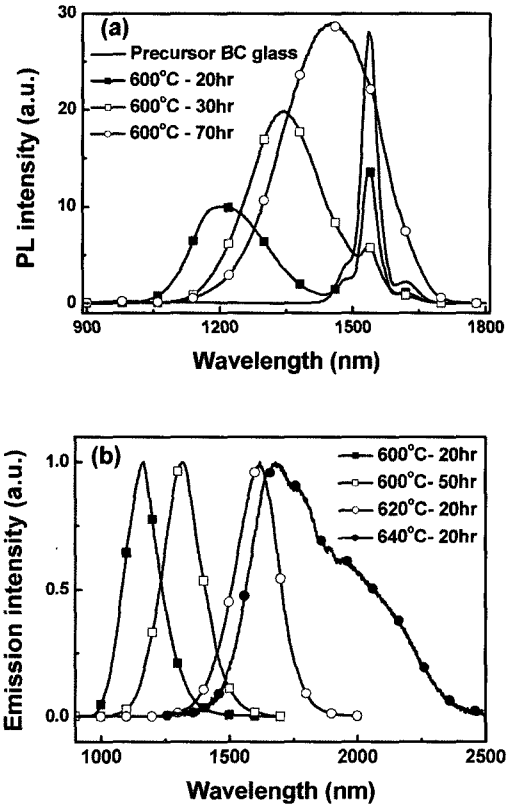

Fig. 6. Room temperature absorption photoluminescence spectra of (a) BC and (b) BZ glass containing PbS QDs. The thermal treatment conditions are indicated in the figure.

4.3 Effect of temperature on the photoluminescence spectra

PL spectra of PbS QDs showed anormalous temperature dependence. Fig. 7 (a) shows the PL spectra recorded at different temperatures using the glass BZ heat-treated at 620°C for 20 h. PL band gradually moved to short wavelength side with increasing temperature, indicating an increase in the effective bandgap energy. Similar phenomena have been reported for semiconductor quantum dots[4,5]. This change in band gap energy with temperature is induced by the thermal expansion of the lattice and electron-phonon coupling[4], and can be simulated using the following empirical formula[3]:

$$E(T) = E_0 + \frac{\alpha T^2}{T + \beta} \quad (6)$$

where E_0 is the energy bandgap at 0 K and T is temperature. α and β are constants that depend on the materials. Temperature dependence of effective bandgap energy calculated from equation (6) was ~ 120 μeV/K, as shown in Fig.7 (b). This value is consistent with that value reported for PbS QDs with a similar size[4].

4.4 Photo-darkening and photo-brightening of PbS QDs

Under continuous excitation condition, photoluminescence intensity of quantum dots either decrease (photo-darkening) or increase (photo-brightening) with time. Photo-darkening and photo-brightening phenomena have been reported for II-VI quantum dots embedded in glass matrix[32,33]. These photo-darkening and photo-brightening phenomena are closely related to the excitation condition, surface states of quantum dots and the surrounding matrix. For example, PbS quantum dots in polymer film at room temperature showed photo-darkening when illuminated in the ambient atmosphere, but resulted in photo-brightening under N_2 environment[34].

On the other hand, the photoluminescence of PbS QDs in borosilicate glasses can be switched from photo-darkened to photo-brightened state as temperature changes. Fig. 8 shows the photo-darkening behavior of PbS QDs in borosilicate glass at room temperature under continuous excitation at 800 nm. This photo-darkening behavior is similar to those observed from other quantum dots in liquids, polymers or glasses[34,35]. As the excitation intensity increased, relative steady-state PL intensity to that at the onset of illumination decreased from 87.5% to 20.0%. This photo-darkening significantly decreased the photoluminescence efficiency.

In addition, photoluminescence changed from photo-darkened state to photo-brightened state as the temperature decreased, as shown in Fig. 9. When temperature was higher than 200K, PbS QDs showed photo-darkening effect, regardless of the excitation intensity. However, when temperature decreased down to 200K for the 200 mW excitation, PL intensity from PbS QDs showed photo-brightening effect, and the degree of brightening increased with a further decrease in temperature. It appeared that photo-brightening was dominant at low temperature, and photo-darkening was enhanced as the temperature increased. With an increase in temperature, the time needed to reach the steady state decreased, indicating that the photo-darkening and photo-brightening were related to phonons.

It has to be emphasized that photo-darkening and photo-brightening observed for PbS QDs in this borosilicate glass were reversible. This reversibility excludes

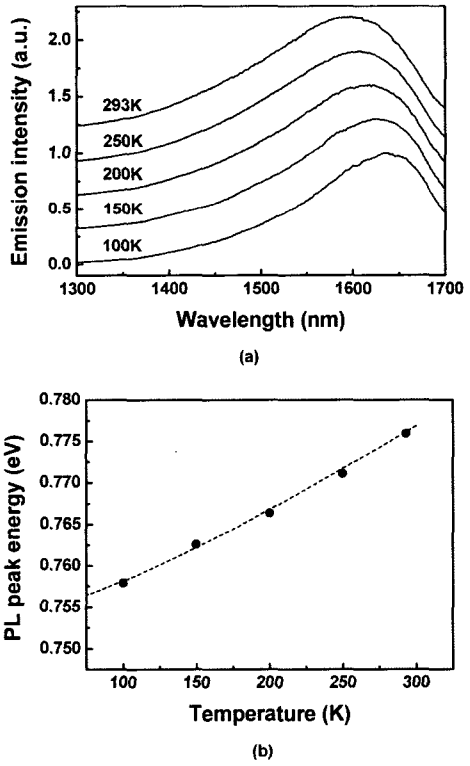

Fig. 7. (a) PL spectra of BZ glass heat-treated at 620°C for 20 h recorded at different temperature. The spectra were shifted vertically for clear presentation. (b) Peak energies of the photoluminescence bands as a function of temperature. Dashed line shows the result of calculation using Eq. (6).

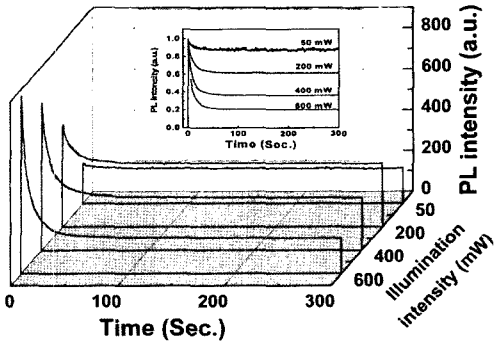

Fig. 8. Changes in the PL recorded from 5.2 nm PbS QDs in borosilicate glass under various illumination intensities. Inset shows steady-state PL intensity normalized to the intensity at the onset of illumination.

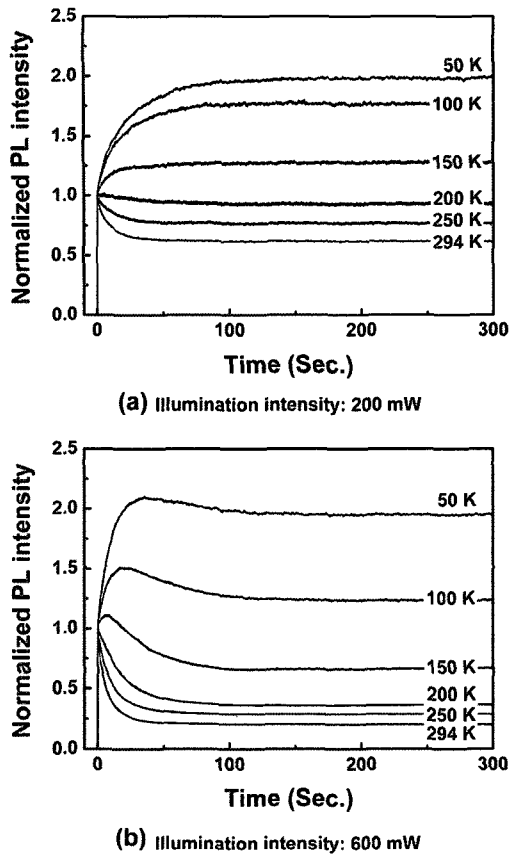

Fig. 9. Change of PL intensity of 5.2 nm PbS QDs recorded at different temperatures with illumination intensity of (a) 200 mW and (b) 600 mW. PL intensity was normalized to the intensity at the onset of illumination.

the possibility of surface of oxidation, which induces irreversible processes. In fact, oxidation of PbS QDs could not occur in the oxide glass matrix, because glass made by melt-quenching methods does not contain free oxygen or moisture. Ionization of QDs induced by illumination or thermal ejection of charge carriers have been proposed to explain the photo-darkening effect[35,36]. Thermal ejection of charge carrier strongly depends on temperature, while photo-ionization does on excitation intensity. Since the photo-darkening of PbS QDs was dependent on temperature and excitation intensity, both thermal ejection and photo-ionization are responsible for the photo-darkening.

Defects in glass matrix formed or activated upon illumination also have an important effect on the photoluminescence intensity of QDs. It has been reported that CdS_xSe_{1-x} QDs showed photo-brightening when irradiated by UV irradiation[33,37]. UV light induced defect centers and carriers trapped at these defect centers were excited into the conduction band of glasses by the excitation light. They finally recombined with surface defects of QDs. This whole process resulted in passivation of the surface defects of QDs and thereby, photoluminescence intensity can be enhanced. Glasses are rich of defects, and these defects can function as sources of charge carriers that eventually passivate the surface defects of QDs, leading to the photo-brightening. In alkali-silicate glasses, defect centers such as E_1 centers are related to the electron-trapping centers at the alkali ions while H_1 centers are associated to the hole-trapping defects of the oxide network[38]. In potassium-silicate glasses, E_1-like centers have binding energies of ~ 1.49 eV at 77 K and 1.61 eV at 210 K. Precursor borosilicate glass used in this work is rich in potassium and photon energy of excitation is 1.55 eV. Thus, electrons or holes initially trapped in the E_1 or H_1-like centers in glasses can easily be excited. Relaxation of these excited electrons or holes passivates the defects at the interface, and results in photo-brightening.

5. Summary

Growth kinetics and optical properties of PbS QDs in the glasses were discussed. High solubility of PbS in phosphate glasses resulted in diffusion controlled growth, and low solubility led to coalescence growth in borosilicate glasses. Hyperbolic-band approximation can predict the exciton energies of PbS QDs of size down to 25 Å, and four-band envelope function formalism provides not only the energy spectrum but also the dipole transition strength and selection rules. Absorption and photoluminescence with large full width at half maximum (>160 nm) in 1~2 μm was achieved through careful control of the thermal treatment condition, promising features for near-infrared applications. Surface defect, temperature and excitation intensity have great effect on the optical properties of PbS QDs. Photoluminescence band shifted to shorter wavelength with decrease in temperature. Photoluminescence of PbS QDs showed photo-darkening and photo-brightening behaviors, and switching between these two states was realized by changing the temperature and excitation intensity.

Acknowledgment

This work was financially supported by the SRC/ERC and STAR programs of MOST/KOSEF (R11-2003-006 and M6-0501-00-0083), Korean Research Foundation Grant funded by the Korea Government (MOEHRD) (KRF-2005-005-J13101) and BK21 Korea.

References

1. M. Jr. Bruchez, M. Moronne, P. Gin, S. Weiss, A. P. Alivisatos, Science 281 (1998) 2013.
2. V. I. Klimov, A. A. Milhailovsky, S. Xu, A. Malko, J, A, Hollingsworth, C. A. Leatherdale, H-J. Eisler, M. G. Bawendi, Science 290 (2000) 314.
3. R. D. Schaller, M. A. Petruska, V. I. J. Klimov, Phys. Chem. B 107 (2003) 13765.
4. L. Bakueva, S. Musikhin, M. A. Hines, T.-W. F. Chang, M. Tzolov, G. D. Scholes, E. H. Sargent, Appl. Phys. Lett. 82 (2003) 2895.
5. R. J. Ellingson, M. C. Beard, J. C. Johnson, P. Yu, O. I. Micic, A. J. Nozik, A. Shabaev, A. L. Efros, Nano Lett. 5 (2005) 865.
6. A. Eychmuller, A. Hasselbarth, L. Katsikas and H. Weller. Bunsenges. Phys. Chem. 95 (1991) 79.
7. Y. Wang, N. Herron, J. Phys. Chem. 95 (1991) 525.
8. M. Mukherjee, A. Datta and D. Chakravorty. J. Mater. Res. 12 (1997) 2507.
9. Y. Chen, Z. Wang, Z. Lin, J. Qian and L. Lin, Appl. Phys. Lett. 68 (1996) 1990.
10. R. S. Kane, R. E. Cohen and R. Silbey. Chem. Mater. 8 (1996) 1919.
11. N. F. Borrelli, D. W. Smith, J. Non-Cryst. Solids, 180 (1994) 25.
12. R. E. de Lamaëstre, H. Bernas, J. Appl. Phys. 98 (2005) 104310.
13. M. Nogami, K. Nagasaka, K. Kotani, J. Non-Cryst. Solids 126 (1990) 92.
14. G. Kellermann, A. F. Craievich, L. C. Barbosa and O. L. Alves, J. Non-Cryst. Solids 293-295 (2001) 517.
15. A. A.Lipovskii, E. V. Kolobkova, A. Olkhovets, V. D. Petrikov, F. Wise, Physica E 5 (2000) 157.
16. R. Kampmanm, R. Wagner, in: Decomposition of Alloys (Oxford Univ. Press, Oxford, 1983).
17. V. P. Koverda et al., Sov. Phys. Crystallogr. 27 (1982) 215.
18. E. M. Lifshits, V. V. Slesov, J. Phys. Chem. Solids 19 (1961) 35.
19. S. Joshi, S. Sen, P. C. Ocampo, J. Phys. Chem. C 111 (2007) 4105.
20. E. M. Lifshitz, L. P. Pitaevskii, Physical Kinetics, Pergamon Press, Oxford, 1981, P.432 (Chapter XII).
21. R. Rossetti, R. Hull, J. M. Gibson, L. E. Brus, J. Chem. Phys. 83 (1985) 1406.
22. Y. Wang, A. Suna, W. Mahler, R. Kasoeski, J. Chem. Phys. 87 (1987) 7315.
23. C. R. Brazier, P. G. Carrick, J. Phys. Chem. 100 (1994) 7928.
24. I. Kang, F. Wise, J. Opt. Soc. Am. B 14 (1997) 1632.
25. A. D. Yoffe, Adv. Phys. 50 (2001) 1.
26. L. Guo, K. Ibrahim, F. Q. Liu, X. C. Ai, Q. S. Li, H. S. Zhu, Y. H. Zou, J. Lumin. 82 (1999) 111.
27. A. A. Patel, F. Wu, J. Z. Zhang, C. L. Torres-Martinez, R. K. Mehra, Y. Yang, S. H. Risbud, J. Phys. Chem. B 104 (2000) 11598.
28. J. Heo, C. Liu, J. Mater. Sci: Mater. Electron. doi:10.1007/s10854-007-9172-1.
29. A. M. Malyarevich, M. S. Gaponeneko, V. G. Savitski, K. V. Yumashev, G. E. Rachkovskaya, G. B. Zakhrevich, J. Non-Cryst. Solids 353 (2007) 1195.
30. N. Daldosso, D. Navarro-Urrios, M. Melchiorri, L. Pavesi, F. Gourbilleau, M. Carrada, R. Rizk, C. Gaecía, P. Pellegrino, B. Garrido, L. Cognolato, Appl. Phys. Lett. 89 (2005) 261103.
31. B. Capoen, A. Martucci, S. Turrell, M. Bouazaoui, J. Mole. Struct. 651-653 (2003) 467.
32. M. Tadaki, H. Akito, S. Tomomi, N. Junya, N. Tetsuro, M. Naoto, Jpn. J. Appl. Phys. 39 (2000) 6290.
33. T. Miyoshi, H. Ohkuni, A. Hirano, T. Suenaga, N. Nozaki, N. Matsuo, J. Mater. Sci. 36 (2001) 493.
34. J. J. Peterson, T. D. Krauss, Phys. Chem. Chem. Phys. 8 (2006) 3851.
35. D. I. Chepic, Al. L. Efros, A. I.Ekimov, M. G. Ivanov, V. A. Kharchenko, I. A. Kudriavtsev, T.V. Yazeva, J. Lumin. 47 (1990) 113.
36. M. Kul, J. L. Coutaz, G. Manneberg, V. Griviscka, Appl. Phys. Lett. 54 (1989) 1830.
37. M. Tadaki, H. Akito, S. Tomomi, N. Junya, N. Tetsuro, M. Naoto, Jpn. J. Appl. Phys. 39 (2000) 6290.
38. J. H. Mackey, H. L. Smith, A. Halperin, J. Phys. Chem. Solids 27 (1966) 1759.